A SiGe Envelope-Tracking Power Amplifier With an Integrated CMOS Envelope Modulator for Mobile WiMAX/3GPP LTE Transmitters

Yan Li, *Student Member, IEEE*, Jerry Lopez, *Student Member, IEEE*, Po-Hsing Wu, Weibo Hu, Ruili Wu, *Student Member, IEEE*, and Donald Y. C. Lie, *Senior Member, IEEE*

***Abstract*—This paper presents a SiGe envelope-tracking (ET) cascode power amplifier (PA) with an integrated CMOS envelope modulator for mobile WiMAX and 3GPP long-term evolution (LTE) transmitters (TXs). The entire ET-based RF PA system delivers the linear output power of 22.3/24.3 dBm with the overall power-added efficiency of 33%/42% at 2.4 GHz for the WiMAX 64 quadrature amplitude modulation (64QAM) and the 3GPP LTE 16 quadrature amplitude modulation, respectively. Additionally, it exhibits a highly efficient broadband characteristic for multiband applications. Compared to the conventional fixed-supply cascode PA, our ET-based cascode PA meets the WiMAX/LTE spectral mask and error vector magnitude spec at close to its $P_{1\mathrm{dB}}$ compression without the need of predistortion. The SiGe PA and the CMOS envelope modulator are both designed and fabricated in the TSMC 0.35-μm SiGe BiCMOS process on the same die. This study represents an essential integration step toward achieving a fully monolithic large-signal ET-based TX for wideband wireless applications.**

***Index Terms*—Differential cascode power amplifier (PA), envelope tracking (ET), high efficiency, linear-assisted switching envelope modulator, long-term evolution (LTE), SiGe BiCMOS, WiMAX.**

I. Introduction

THIRD-GENERATION (3G) cellular services are being deployed on a worldwide basis, along with the higher data rate so-called fourth-generation (4G) wireless standards such as WiMAX/WiBro and 3GPP long-term evolution (LTE). The true 4G Advanced LTE service is expected to be offered in a few years, promising maximum download speed of 1 Gb/s. The IEEE 802.11n wireless local area network (WLAN) standard that utilizes the multiple input/multiple output (MIMO) antenna technology already achieves a maximum download speed of over 150 Mb/s in real-life Wi-Fi certified products today. These 3G/4G/WLAN wireless services require wide bandwidths and spectrally efficient modulation schemes with larger peak-to-average ratios (PARs) than their second-generation (2G)/2.5G counterparts. Therefore, it is becoming much more challenging to design highly efficient and linear transmitters (TXs) for portable wideband wireless applications.

The RF power amplifier (PA) tends to be the most power-hungry block for a typical mobile TX (e.g., in [1], the PA consumes 78% power of the entire TX). The nonconstant-envelope modulated signals with the inherent high PAR and wide bandwidth require highly linear PAs having very low signal distortion. One way for the PA to satisfy the stringent linearity requirements is to *back off* from its compression region. This is a major bottleneck for realizing highly efficient mobile TXs, since the power-added efficiency (PAE) of the PA reduces dramatically in back-off mode, as opposed to the PAE of saturated PAs operating at peak output power. For example, many commercially available PAs based on a III–V compound semiconductor can produce saturated output power over 30 dBm with peak PAEs greater than 45%, but they need 3–4-dB back-off from the $P_{1\mathrm{dB}}$ compression points to meet the 3GPP LTE linearity specs, resulting in $\sim$35% PAE in the best case for the LTE quadrature phase-shift keying (QPSK) modulation (PAR of $\sim$6.5 dB).[1] Moreover, due to higher PAR of WiMAX over LTE, PAs would need more back-off (i.e., usually $\sim$6–8 dB) to meet the stringent WiMAX linearity specs, leading to even lower PAE (e.g., only $\sim$20% PAE[2]). Likewise, in the recent literature, CMOS PAs with on-chip transformers have successfully delivered over 30-dBm saturated power with the best PAE value of $\sim$50% [2]–[9], but they need a large back-off to meet the linearity specs for high PAR signals resulting in a greatly reduced PAE (e.g., only $\sim$10%–20% for WiMAX/WLAN [4], [8], [10]). A state-of-the-art linear SiGe dual-standard LTE/WiMAX PA has been recently reported with a saturated power of $\sim$30 dBm and a peak PAE of $\sim$30%, but again its PAE is less than 20% once backed off 5 dB to satisfy the WiMAX linearity requirements [11].

To boost the PA efficiency for high PAR signals, envelope-tracking (ET) or envelope-elimination-and-restoration (EER) TX architectures can be very effective as the PA supply voltage is modulated according to the instantaneous output

Manuscript received March 02, 2011; revised July 08, 2011; accepted July 28, 2011. Date of publication September 15, 2011; date of current version October 12, 2011. This work was supported by the Industrial Technology Research Institute (ITRI), Taiwan.

Y. Li, J. Lopez, W. Hu, R. Wu, and D. Y. C. Lie are with the Department of Electrical and Computer Engineering, Texas Tech University, Lubbock, TX 79409 USA (yan.li@ttu.edu; yan.li.ttu@gmail.com; donald.lie@ttu.edu).

P.-H. Wu was with the Department of Electrical and Computer Engineering, Texas Tech University, Lubbock, TX 79409 USA. He is now with Diodes Taiwan Inc., Hsinchu 300, Taiwan.

Color versions of one or more of the figures in this paper are available online at http://ieeexplore.ieee.org.

Digital Object Identifier 10.1109/TMTT.2011.2164550

[1]For example: [Online]. Available: http://www.anadigics.com//products/view/alt6713

[2]For example: [Online]. Available: http://www.analog.com/static/imported-files/data_sheets/ADL5571.pdf

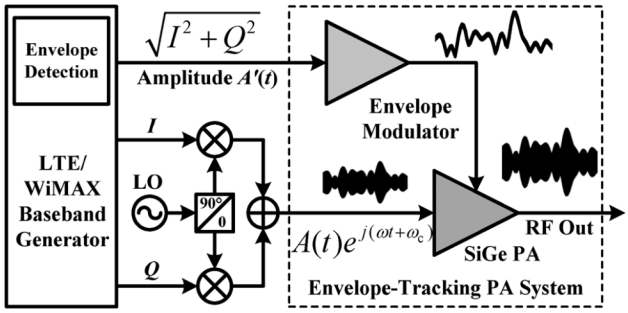

Fig. 1. Simplified block diagram of the ET-based RF TX in this work.

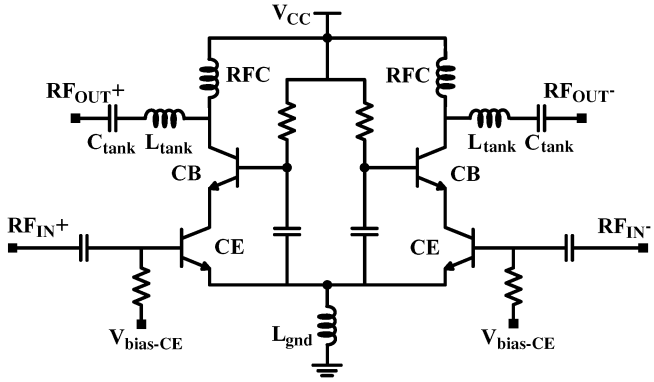

Fig. 2. Simplified circuitry schematic of the differential cascode SiGe PA.

power [12]. ET/EER-based TXs have recently demonstrated excellent overall system efficiency and linearity for several 3G/4G applications [12]–[22], [38]–[42]. For Si-based PAs, when the supply voltage is modulated by high PAR envelope signals, the power transistor is highly stressed as the collector/drain voltage swing in the saturated PA can be $\sim 2\times$–$4\times$ of its supply voltage [23]. The cascode PA configuration, therefore, has been used to relieve the voltage stress on the power devices [24], [25]. In [5]–[7], the cascode PAs showed the potential effectiveness in EER-based polar TXs, delivering $P_{\rm out}$ over 30 dBm for some low PAR narrowband applications (e.g., EDGE and GSM); in the aforementioned, the PA linearity was not a topic of emphasis.

In this paper, as shown in Fig. 1, we focus on the ET-based TX system for high PAR wideband wireless applications. A cascode SiGe PA is utilized in the system and modulated by a CMOS envelope modulator. A discussion on the efficiency enhancement and the necessary methodology for improving linearity simultaneously will be presented. The SiGe PA and the CMOS envelope modulator have been integrated on the same die and evaluated on the test bench for WiMAX/LTE modulations. This ET-based PA system is an essential step toward achieving a fully integrated large-signal ET-based TX for wideband wireless applications.

The outline of this work is as follows. Section II presents the differential cascode SiGe PA design and the approach to improve its linearity in the proposed ET-based TX system. Section III discusses design insights of the monolithic linear-assisted switching envelope modulator for high PAR signals. In Section IV, WiMAX 64 quadrature amplitude modulation (64QAM) 5-MHz and LTE 16 quadrature amplitude modulation (16QAM) 5-MHz signals are used to demonstrate the high efficiency and good linearity performances of our ET-based PA system. A conclusion is drawn in Section V.

II. Differential Cascode SiGe PA

A. Cascode PA Design and Continuous Wave (CW) Measurement

The simplified schematic of our differential cascode PA is shown in Fig. 2. The differential topology can reduce the second harmonics and also the parasitic ground inductance at RF, which can hurt the gain and PAE of a PA significantly [21]. A high-f_T low-$\rm BV_{CEO}$ bipolar device is utilized in the common-emitter (CE) stage, while a high-$\rm BV_{CEO}$ low-f_T bipolar device is used in the common-base (CB) stage. The CB transistor is *self-biased* for the linearity improvement in the ET system and the details will be discussed in Section II-B. The RF chokes (RFCs) were implemented by bond wires and also with off-chip inductors to achieve the minimum inductor losses for highest PAE. The output tank inductors were also implemented by bond wires. Off-chip passive components were placed on an FR4 printed circuit board (PCB). This PA requires two off-chip baluns to convert the differential signal into a single-ended signal and vice versa. The balun loss was de-embedded from the measurement results.

The definition of *broadband* PAs in [27]–[29] is based on the PA's ability to achieve a similar compressed output power across the band of interest, while maintaining its high PAE. The RFC and output *LC* tank are the only frequency-selective components in our cascode PA circuit. When our cascode PA was optimized with a low-Q output *LC* tank, it can demonstrate a fairly constant compressed output power with high efficiency over a wide bandwidth [27]. Fig. 3 shows the CW measurement results of our differential cascode SiGe PA driven into $P_{\rm 1dB}$ compression at different frequencies. The $P_{\rm 1dB}$ output power maintained around 24–25.5 dBm with PAE of 48%–60% from 0.8 to 2.6 GHz. These performances were achieved by testing several PA dies with the same tuning for the best possible bandwidth over the desired frequency range. This testing methodology ensured the performance reproducibility across several units. Furthermore, the PA remained highly stable across the frequency bands of interest.

Since the traditional S-parameters measurement is based on the small-signal assumption, it is not very useful to characterize the input matching for a large-signal PA. The PA input matching in this work, therefore, is assessed by the frequency response of the input reflection at several input power levels. Fig. 4 shows the input reflection remains stable across the entire band (i.e., 0.8–2.6 GHz) with only a $\pm$1.5-dB variation, presenting well-defined input impedance. This characteristic of a stable input matching in addition to a constant output $P_{\rm 1dB}$ (refer to Fig. 3) confirms the broadband nature of our cascode PA. Also, even though the cascode PA was driven into compression, the input reflection was not highly affected. For example, the PA was driven into compression states at 8-dBm input power at frequencies below 2.1 GHz, but the change of input reflection

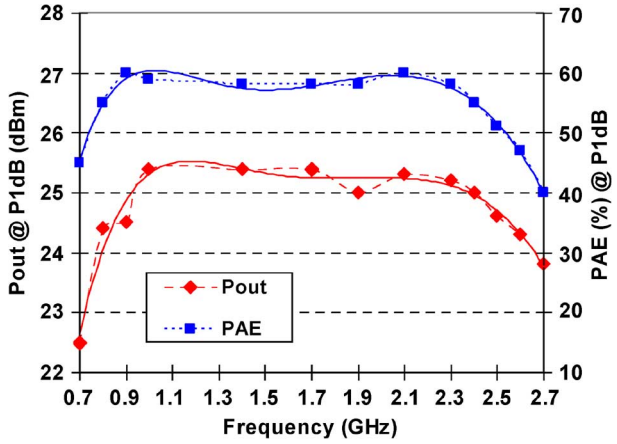

Fig. 3. Measured frequency response of the $P_{1\mathrm{dB}}$ output power and PAE (at $P_{1\mathrm{dB}}$) of the differential cascode PA in CW mode; supply voltage V_{CC} = 3.6 V.

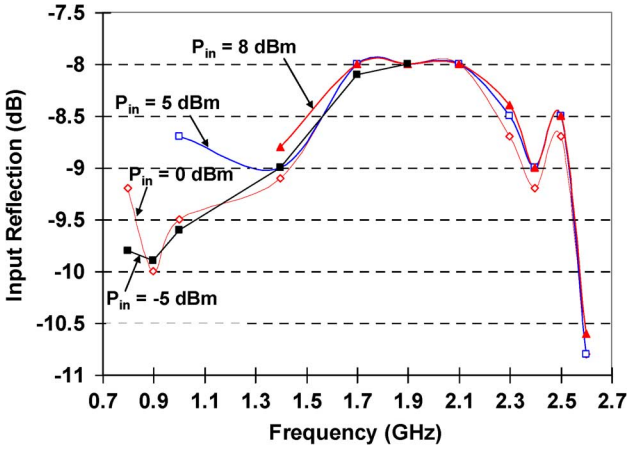

Fig. 4. Measured frequency response of the input reflection at different input power levels.

is small, as shown in Fig. 4. This demonstrates a good isolation between the input and output ports because of the cascode topology used.

B. Linearity Enhancements for Cascode PAs in ET

The linearity performance of a cascode PA is generally worse compared with its CE/source PA counterparts [30]. For the optimal use of cascode PAs in an ET-based TX system, we will investigate two cases, which concern: 1) constant biasing of the CB transistor and 2) self-biasing of the CB transistor. Fig. 5(A) and (B) shows the simplified schematics of the constant biased cascode PA and the self-biased cascode PA, respectively. The equivalent R_{ON} (i.e., the "on-resistance") of the CB transistor was simulated and shown in Fig. 6 for the above two cases. The R_{ON} of the constant biased CB transistor linearly decreases from 52 to 11 Ω as the supply voltage V_{CC} decreases from 4.2 to 0.8 V, while the R_{ON} of the self-biased CB transistor varies very little at V_{CC} above 1.9 V (i.e., from 24 to 26 Ω), and starts to rapidly increase once V_{CC} is below 1.9 V.

In our ET system implementation, the self-biased cascode PA is modulated by a dc-shifted envelope signal (i.e., we refer to this as "envelope shifting"). The minimum envelope level is set

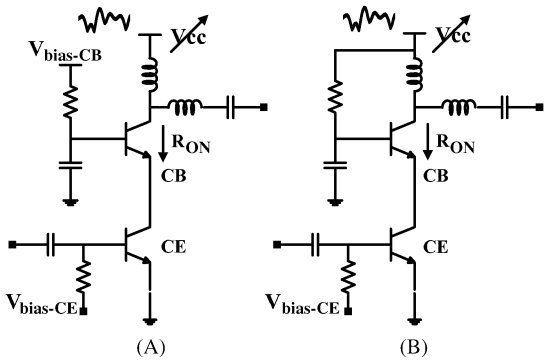

Fig. 5. Simplified schematics. (A) Constant biased cascode PA. (B) Self-biased cascode PA.

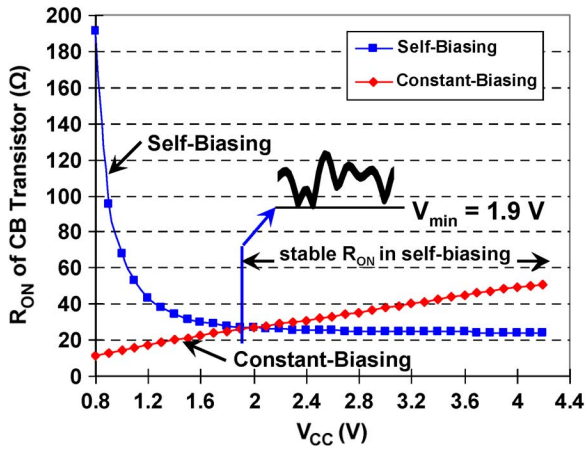

Fig. 6. Simulated R_{ON} of the self-biased CB transistor and the constant biased CB transistor for our cascode SiGe PAs.

to 1.9 V. Meanwhile, the ac magnitude of the envelope signal is reduced to avoid possible clipping due to the swing limitation of the envelope modulator. The ac magnitude attenuation is dependent on the PAR of the envelope signal. Fig. 7 illustrates the envelope-shifting method for WiMAX 64QAM 5 MHz, presenting a decreased PAR for the shifted envelope. After the shifted envelope is applied to the self-biased cascode PA, the R_{ON} of the CB transistor will remain stable throughout the swing range of the modulated supply voltage (V_{CC}). Please note that this topology is different from the work reported in [5]. In [5], the constant biased cascode PA was used in a conventional EER system to achieve high efficiency when its modulated supply voltage approached 0. However, in this study, linearity is one of our main concerns for realizing a highly efficient ET-based TX with high PAR wideband signals, therefore the self-biased cascode PA is adopted here with the envelope-shifting method.

To validate our approach for improving the cascode PA linearity in the ET system, we simulated the entire ET-based TX system using our differential cascode SiGe PA in Agilent's Advanced Design System (ADS). The realistic SPICE models provided by the TSMC 0.35-μm SiGe BiCMOS design kit were used for the PA. The RF/analog/digital system co-simulation methodology was described in detail in [31] and it was also applied in this study. The WiMAX 64QAM 5-MHz signal was applied to the system. Fig. 8 shows the simulated output spectra of

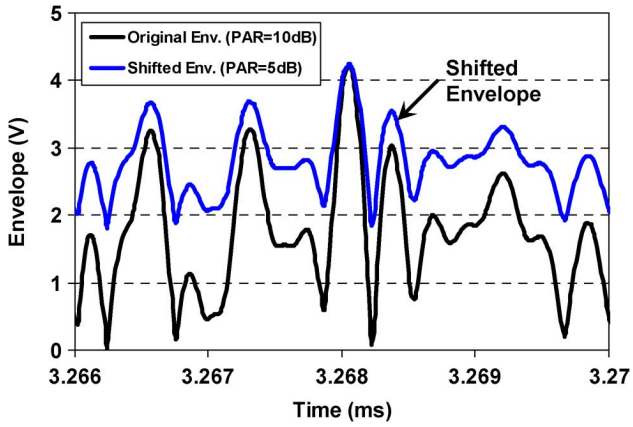

Fig. 7. Simulated envelope signals before/after envelope shifting for the WiMAX 64QAM 5-MHz signal.

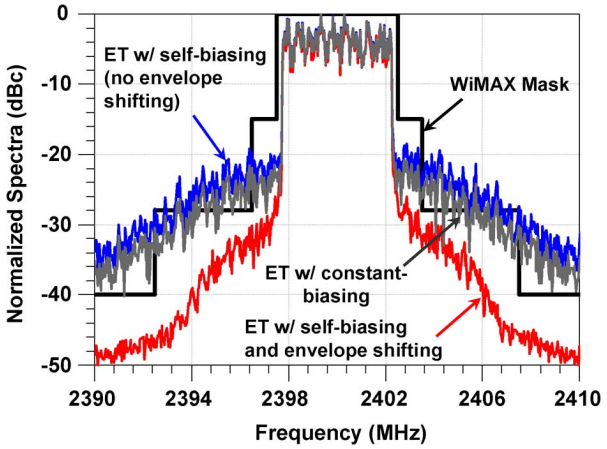

Fig. 8. Simulated output spectra of the ET-based TX system using constant biased cascode PA and self-biased cascode PA with/without envelope shifting. The ideal envelope modulator was used in the simulation to highlight the effects of envelope shifting. The WiMAX 64QAM 5-MHz signal at 2.4 GHz was applied to the system.

the ET-based TX system using the constant biased cascode PA and the self-biased cascode PA. The latter case was simulated with and without the envelope shifting. To highlight the effects of envelope shifting, an ideal envelope modulator (i.e., a distortionless gain block in ADS) was used, in this particular simulation, to remove distortions from the amplitude path. It is clearly seen that the output spectrum of the self-biased cascode PA with envelope shifting has the lowest distortion. This suggests that by keeping $R_{\rm ON}$ of the CB transistor stable improves the linearity of the cascode PA in ET systems for nonconstant-amplitude modulated signals.

Once the envelope shifting is optimized for cascode PA linearity, the PA efficiency is measured in the CW mode at different V_{CC} levels to mimic the PA response in the ET system. Fig. 9 shows that the PAE trajectory of the ET-based PA tracks the peak PAE points (see the dashed line). As V_{CC} is modulated from 1.8 to 4.2 V, the PAE of the ET-based PA varies between 53%–61%. Fig. 9 also shows the load impedance $R_{\rm load}$ (seen by the envelope modulator) under the modulated V_{CC}. It is calculated from the dc supply voltage and the measured current consumption of the PA at each peak PAE [15]. $R_{\rm load}$ stays constantly at $\sim 20\ \Omega$, when V_{CC} is swept from 1.8 to 4.2 V.

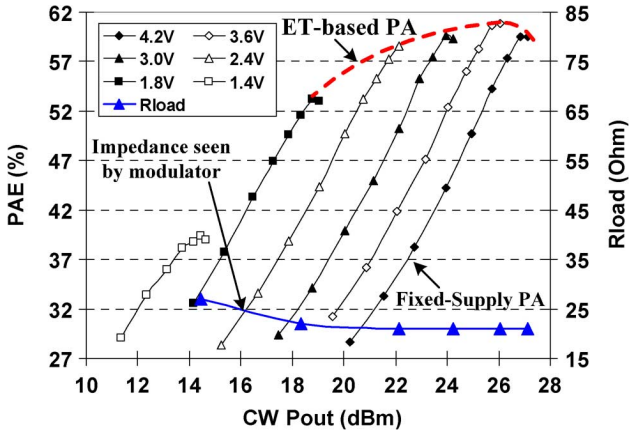

Fig. 9. Measured PAE values of the self-biased monolithic differential cascode SiGe PA and the load impedance seen by the envelope modulator at different V_{CC} in the CW mode.

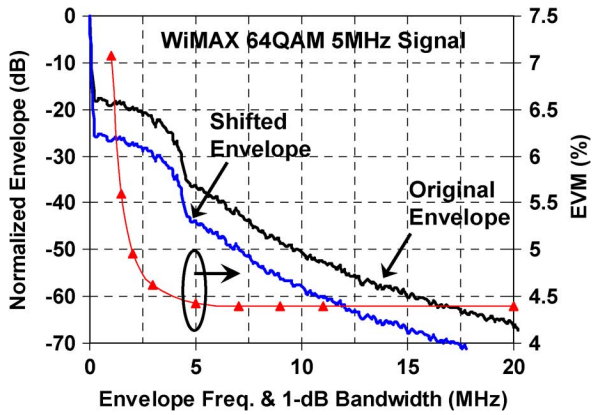

Fig. 10. Normalized envelope spectra and simulated EVM versus the 1-dB bandwidth of the envelope modulator for the WiMAX 64QAM 5-MHz signal. Realistic SPICE model was used for the differential cascode SiGe PA. A fourth-order Butterworth LPF was used to mimic the envelope modulator. PA output power $=$ 23 dBm (i.e., at $P_{\rm 1dB}$).

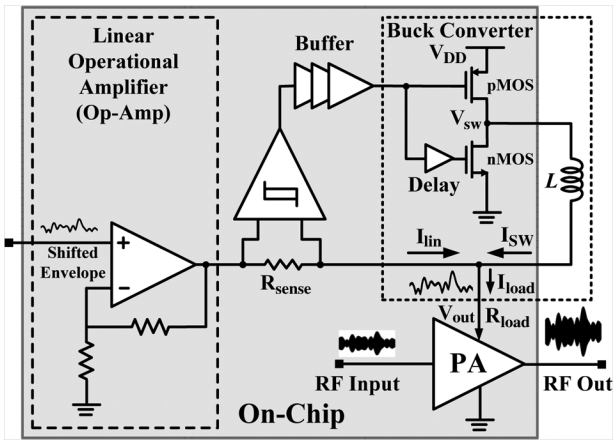

Fig. 11. Simplified block diagram of our CMOS envelope modulator with its connection to the differential cascode SiGe PA on the same die.

III. Linear-Assisted Switching Envelope Modulator

A. Bandwidth Requirement of Envelope Modulator

Proper envelope modulator design is critical to achieve the best overall TX system efficiency and linearity performance. The finite bandwidth and associated group delay of envelope

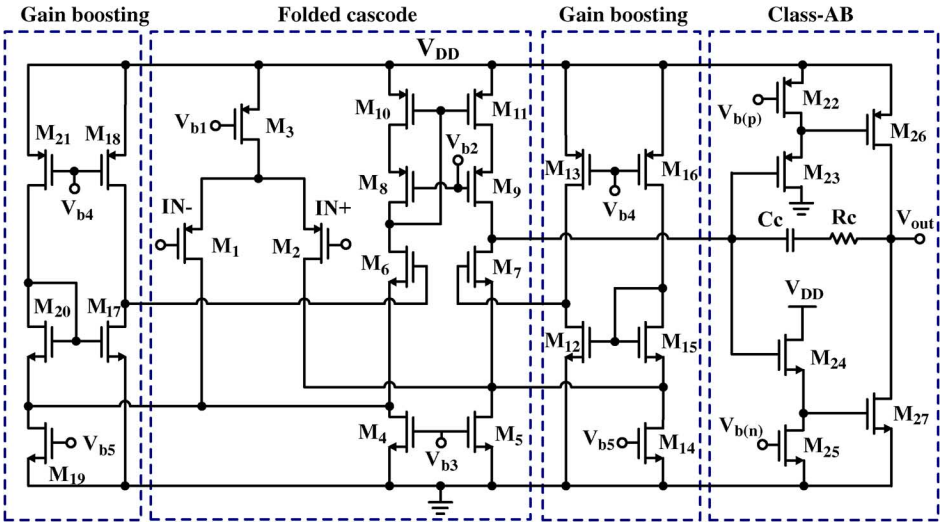

Fig. 12. Simplified circuit schematic of the linear Op-Amp with a class-AB output stage used in our CMOS envelope modulator design.

modulators are large contributors of nonlinearity sources in ET/EER-based PA systems [32].

The envelope spectra of the WiMAX 64QAM 5-MHz signal are shown in Fig. 10. Due to the nonlinear Cartesian-to-polar transformation, the bandwidth of the original envelope signal expands up to 7.2 MHz to contain 99.9% envelope power [33]. However, the envelope-shifting method in our ET system (as described in Section II) alleviates the bandwidth requirement of the envelope modulator. This is because the envelope shifting moves high-frequency contents into dc (see Fig. 10). Additionally, compared with EER systems, the ripple and accuracy of the envelope modulator are less critical in ET systems so that the required filtering and timing alignment are considerably relaxed [14], [20].

To investigate the bandwidth requirement of the envelope modulator in our ET-based PA system, we simulated the system with the WiMAX 64QAM 5-MHz signal in the ADS RF/analog/digital co-simulation platform. A fourth-order Butterworth low-pass filter (LPF) was used to mimic the finite bandwidth of the envelope modulator. The group delay caused by the LPF was compensated at the RF path, which is dependent on the bandwidth of the filter. The realistic SPICE models were again used for our differential cascode SiGe PA. The simulated error vector magnitude (EVM) values against different 1-dB bandwidths of the envelope modulator are also plotted in Fig. 10. Here, the 1-dB bandwidth is defined as the frequency where the gain of the envelope modulator decreases by 1 dB. The PA was driven into its $P_{1\mathrm{dB}}$ compression at 2.4 GHz (i.e., $P_{\mathrm{out}} = 23$ dBm). As seen from Fig. 10, EVM stays constant once the 1-dB bandwidth of the envelope modulator is larger than 7 MHz. The distortion in this analysis did not include the contribution from the envelope clipping. Considering the swing limitation in real situations, we estimate the sufficient 1-dB bandwidth of the envelope modulator would be $\sim \times 1.5$–$\times 2$ of the signal bandwidth for our ET system.

B. Envelope Modulator Design and Implementation

In this study, our envelope modulator utilizes a hybrid configuration with a linear Op-Amp and a switching buck converter, as shown in Fig. 11 [14], [15], [17], [34]. The highly efficient switching stage supplies most of the load current. Meanwhile, the wideband linear Op-Amp stage not only compensates the difference between the desired load current (I_{load}) and the switching current (I_{SW}), but also attenuates the switching ripples. The switching stage is controlled by sensing the output current of the linear stage (I_{lin}) and comparing it with the threshold level of a hysteretic comparator. The value of R_{sense} is chosen to be 1 Ω on-chip. The efficiency of the whole envelope modulator is a combination of the switching stage efficiency (η_{SW}) and the linear stage efficiency (η_{lin}), as expressed by

$$\eta_{\text{env-mod.}} = 1/\left[\alpha/\eta_{\mathrm{SW}} + (1-\alpha)/\eta_{\mathrm{lin}}\right] \tag{1}$$

where α is the ratio of the dc content to the total envelope power [35].

The monolithic envelope modulator was also designed in the TSMC 0.35-μm BiCMOS process, but no bipolar devices were used in this particular block. The linear stage (shown in Fig. 12) consists of a folded cascode amplifier with gain-boosted stages and a class-AB output stage. The open-loop gain of the boosted-folded cascode amplifier was set to 75 dB to meet the slew-rate requirement needed for the WiMAX/LTE envelope signals. Additionally, the zero-pole doublet formed by gain-boosting stages ($\mathrm{M}_{12\text{-}16}$ and $\mathrm{M}_{17\text{-}21}$) was pushed roughly to about one decade above the required bandwidth (i.e., in this case, $\sim$70 MHz) to avoid large resonance and stability issues. The voltage gain of the linear Op-Amp in feedback mode is 6 dB.

The hysteretic current control is implemented by a high-gain open-loop comparator with an internal positive feedback. Its simplified circuitry schematic is shown in Fig. 13, consisting of a positive gain stage, a level shifter, and a three-stage buffer. Assuming an ideal bias current is provided, the constant hysteresis window V_h can be expressed as

$$|V_h| = |V_{\mathrm{GS2}} - V_{\mathrm{GS1}}| = \left|\frac{2I_2}{g_{m2}} + V_{T2} - \frac{2I_1}{g_{m1}} - V_{T1}\right|. \tag{2}$$

In this study, to obtain a stable hysteresis window, a cascode current sink $(\mathrm{M}_5, \mathrm{M}_8)$ is used to increase the output resistance, resulting in a more constant bias current. The determination of

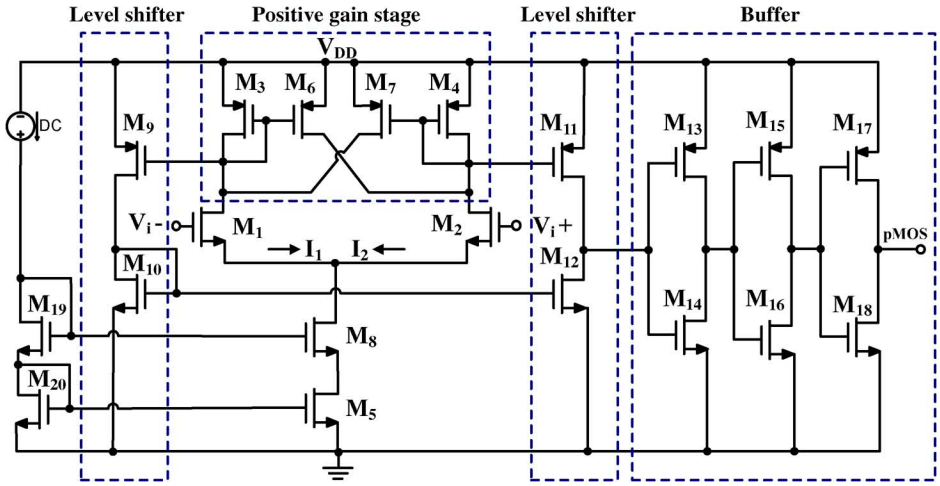

Fig. 13. Simplified circuit schematic of the hysteretic comparator with a three-stage buffer used in our CMOS envelope modulator design.

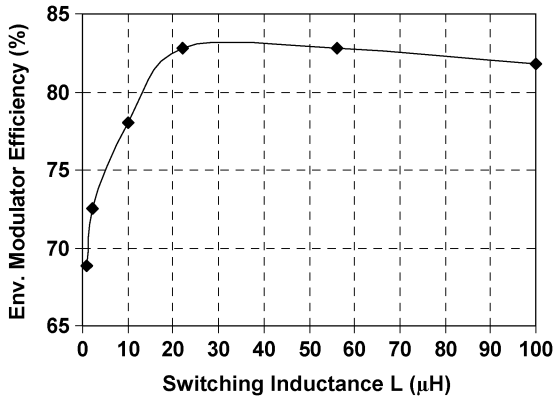

Fig. 14. Measured efficiency of the CMOS envelope modulator for the shifted envelope of WiMAX 64QAM 5-MHz; supply voltage $V_{DD} = 4.2$ V.

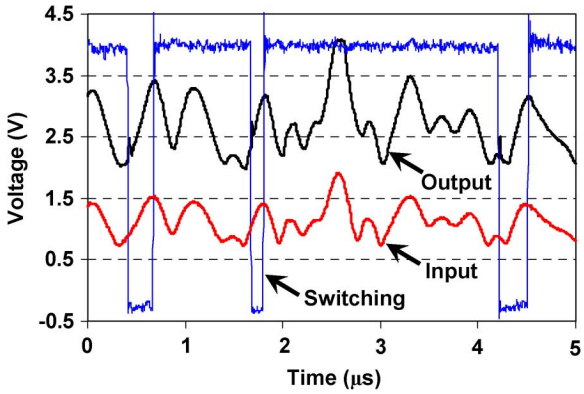

Fig. 16. Measured transient responses of the envelope modulator for the shifted envelope of the WiMAX 64QAM 5-MHz; voltage gain of 6 dB.

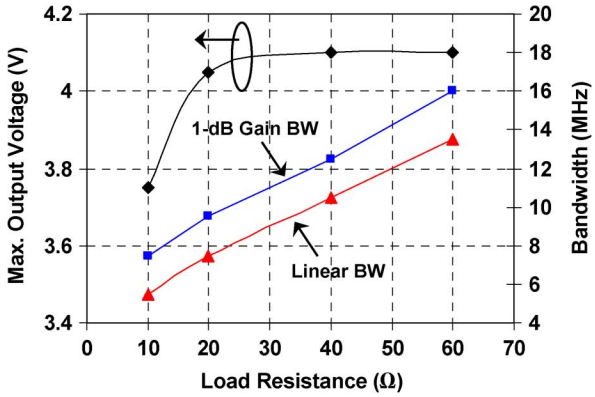

Fig. 15. Measured bandwidths and maximum output voltages of the CMOS envelope modulator at different load resistances; supply voltage $V_{DD} = 4.2$ V.

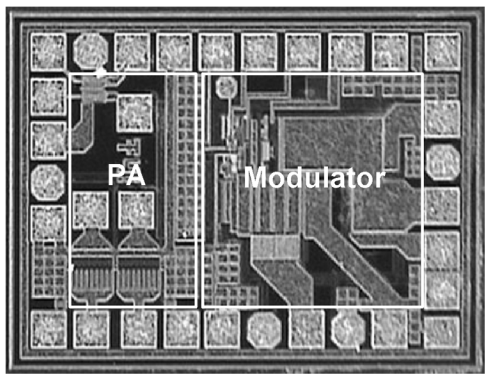

Fig. 17. Chip micrograph of the ET-based PA system (1.1×1.5 mm^2).

the hysteresis window V_h needs to consider the tradeoff between the signal fidelity and the switching frequency. A smaller V_h will lead to a smaller error, but a larger switching frequency (thus, higher switching loss), as reported by [17]. In our case, a 10-mV hysteresis window was used.

The switching stage is realized by a buck converter (see Fig. 11). The pMOS and nMOS of the buck converter were sized to supply the necessary current to the PA, while keeping a minimal conduction loss. In our case, the nMOS is 7 mm $\times$ 0.4 μm and the pMOS is 20 mm $\times$ 0.4 μm. The pMOS and nMOS should be turned "on/off" simultaneously to prevent the shoot-through loss. Since the crossover time between the pMOS turning off and the nMOS turning on is $\sim$2 ns, as indicated in the SPICE simulation, an extra buffer is required to introduce the additional dead time for the nMOS (shown in Fig. 11).

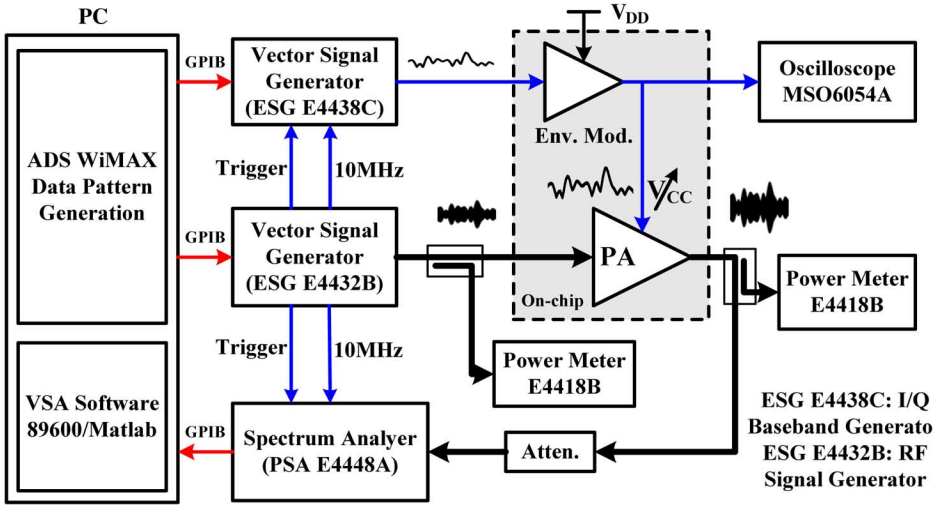

Fig. 18. Test bench setup to characterize our ET-based PA for WiMAX/LTE.

The inductor L of the buck converter was implemented off-chip. The choice of the inductance value can have a major impact on the efficiency of the envelope modulator. When L is chosen on the high side, the buck converter cannot deliver a large current at high frequencies so the linear Op-Amp has to deliver the remaining signal, and this will lead to higher power dissipation. On the other hand, a too low value of L results in a high switching frequency and large switching losses. Additionally, too small of L causes switching ripples at higher frequency and requires wider bandwidth and lower impedance from the linear Op-Amp, making the Op-Amp design very challenging [14], [15], [34].

The optimal inductance L can be chosen at the point where the average slew rate of the switching current $(I_{\rm sw})$ is equal to the average slew rate of the load current $(I_{\rm load})$, expressed as

$$\overline{\left|\frac{dI_{\rm sw}}{dt}\right|}=\overline{\left|\frac{dI_{\rm load}}{dt}\right|}=\frac{2}{L}\left(V_{\rm ave}-\frac{V_{\rm ave}^2}{V_{DD}}\right)=\frac{1}{R_{\rm load}}\overline{\left|\frac{dV_{\rm out}}{dt}\right|} \tag{3}$$

where $V_{\rm out}$ is the output voltage and $V_{\rm ave}$ is the average level of $V_{\rm out}$. In our case, the average slew rate of $V_{\rm out}$ is $\sim 3.5\ {\rm V}/\mu{\rm s}$, $V_{\rm ave}$ is ~2.9 V, and $R_{\rm load}$ is 20 Ω for our shifted 64QAM 5-MHz orthogonal frequency division multiplexing (OFDM) envelope signal, and the calculated L from (3) is $\sim$ 12 μH. To verify our decision of L, we also measured the efficiency of the envelope modulator using different off-chip inductors, as plotted in Fig. 14. The optimal L for achieving maximum efficiency is found to be 22–56 μH in the measurement, which is higher than our calculation. The discrepancy is likely due to the inaccuracy of the theoretical model for handling high PAR wideband signals. We chose L of 22 μH for our final design, which provides high efficiency with good signal fidelity.

C. Maximum Output Voltage and Bandwidth Versus $R_{\rm load}$

A major design concern regarding to the monolithic ET-based system implementation is the $R_{\rm load}$ that depends on the PA operating regions. The maximum output voltage $(V_{\rm out})$ and bandwidth of the envelope modulator are directly related to $R_{\rm load}$. Fig. 15 shows the measured linear bandwidth, 1-dB bandwidth, and the maximum $V_{\rm out}$ with different $R_{\rm load}$ values. This linear bandwidth is defined by where the gain response decreases by a mere 0.1 dB. The bandwidths and the maximum $V_{\rm out}$ increase with larger $R_{\rm load}$. The minimum $R_{\rm load}$ was previously found to be $\sim$ 20 Ω for our differential cascode PA (see Fig. 9). Based on Fig. 15, our monolithic envelope modulator can provide 1-dB bandwidth above 10 MHz, which satisfies the required bandwidth, as discussed in Section III-A. A maximum $V_{\rm out}$ above 4 V can also be achieved, giving enough headroom to deliver a sizable PA output power (i.e., for $R_{\rm load} > 16\ \Omega$). For wider bandwidth envelope signals, using smart algorithms to reduce the envelope bandwidth, such as [36], could be effective.

Fig. 16 shows the measured input, output, and switching waveforms of our CMOS envelope modulator for the WiMAX 64QAM 5-MHz signal. The switching waveform was measured at the drain of the pMOS (refer to Fig. 11). The output signal shows good fidelity compared with the input signal. The output voltage range is from 1.9 to 4.05 V with the load resistance of 20 Ω under a 4.2-V supply voltage.

IV. System Experimental Results

The entire ET-based PA system was fabricated in the commercially available TSMC 0.35-μm SiGe BiCMOS process. Fig. 17 shows the chip micrograph with a total chip area (including pads) of 1.1 × 1.5 mm^2. The test bench setup of our ET-based PA system is shown in Fig. 18. The WiMAX/LTE envelope and baseband signals are generated by Agilent's ADS and then downloaded into Agilent ESG 4438C and ESG 4432B, respectively. The envelope shifting is realized inside the ESG 4438C. The RF signal from the PA is down converted and digitized in the spectrum analyzer and received by the vector signal analysis (VSA) software for linearity analysis. The spectrum analyzer and two signal generators are synchronized using a data pattern trigger. The static delay between the RF path and amplitude path is compensated in ADS. The entire ET-based PA system is operated under the supply voltage (V_{DD}) of 4.2 V, sufficiently large not to cause considerable envelope clipping from the envelope modulator. No predistortion was applied to the system for the data reported in this work. The overall PAE

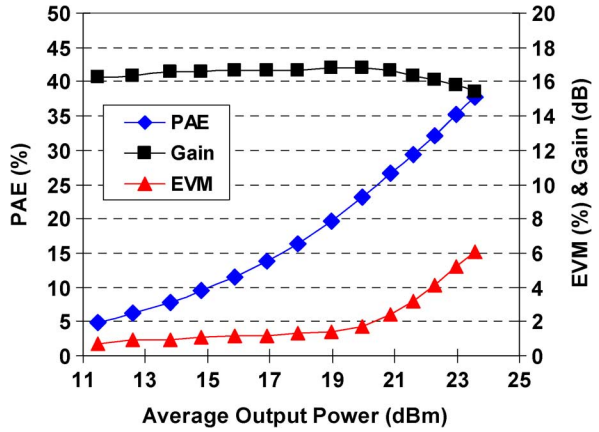

Fig. 19. Measured EVM, gain, and overall PAE of the monolithic ET-based PA system for WiMAX 64QAM 5-MHz signals at 2.4 GHz.

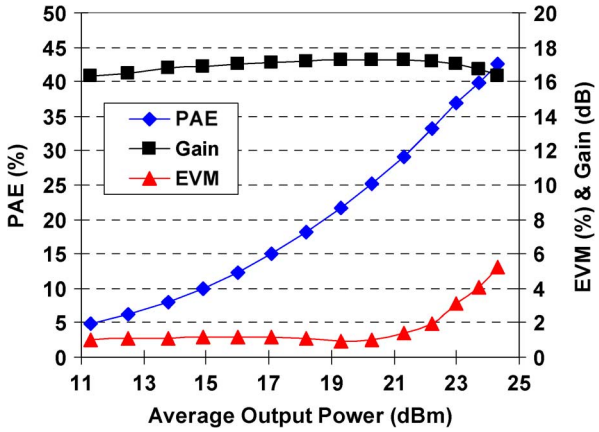

Fig. 20. Measured EVM, gain, and overall PAE of the monolithic ET-based PA system for LTE 16QAM 5-MHz signals at 2.4 GHz.

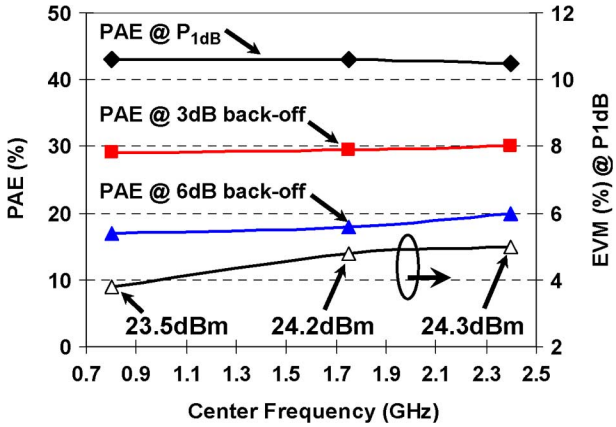

Fig. 21. Measured overall PAE and EVM (at $P_{1\mathrm{dB}}$) of the ET-based PA system for the LTE 16QAM 5-MHz signal at 0.8/1.75/2.4 GHz.

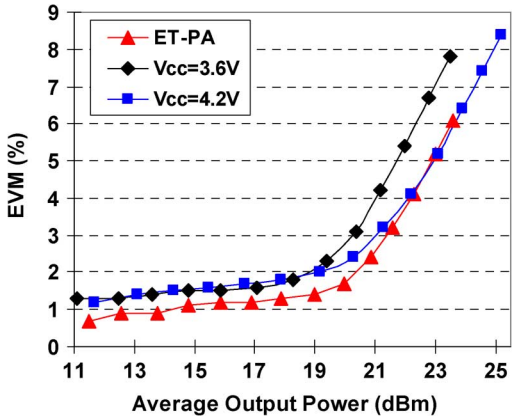

Fig. 22. Measured EVM of the ET-based PA ($V_{DD} = 4.2$ V) and the fixed-supply PA ($V_{CC} = 3.6$ V/4.2 V) for the WiMAX 64QAM 5-MHz signal at 2.4 GHz. No predistortion applied to either the ET-based PA or the fixed-supply PA.

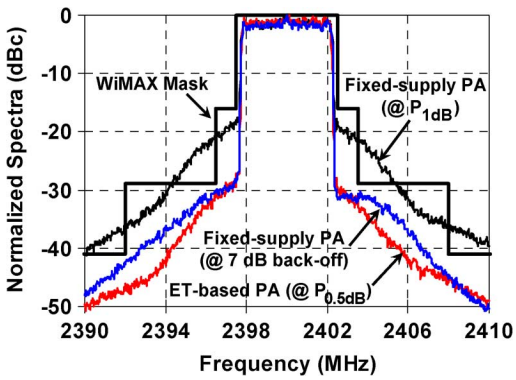

Fig. 23. Measured output spectra of the ET-based PA versus the fixed-supply PA for the WiMAX 64QAM 5-MHz signal at 2.4 GHz.

TABLE I
PERFORMANCE COMPARISON OF OUR ET-BASED PA SYSTEM VERSUS THE FIXED-SUPPLY CASCODE PA FOR THE WiMAX 64QAM 5-MHz SIGNAL AT 2.4 GHz

	Fixed-supply PA ($P_{1\mathrm{dB}}$)	Fixed-supply PA (7 dB back-off)	ET-based PA ([1]$P_{0.5\mathrm{dB}}$)
V_{DD}/V_{CC}	4.2 V	4.2 V	4.2 V
Ave. P_{out}	25 dBm	18 dBm	22.3 dBm
PAE	48%	*22%*	*33%*
Gain	16 dB	17 dB	16 dB
[2]EVM	8.4%	2%	4.2%
Pass Mask?	No	Yes	*Yes*

1. $P_{0.5\mathrm{dB}}$ means the ET-based PA is 0.5 dB compressed at the average P_{out} of 22.3 dBm (not reaching $P_{1\mathrm{dB}}$ yet, as can be seen from Fig. 19).
2. The EVM spec is 5% for the WiMAX 64QAM standard; no predistortion applied to either the ET-based PA system or the fixed-supply PA.

reported below includes the power consumption incurred by the envelope modulator.

A. Linearity and Efficiency Characterizations

Fig. 19 shows the measured EVM, gain, and overall PAE of the monolithic ET-based PA system for the WiMAX 64QAM 5-MHz signal at 2.4 GHz (PAR $\sim$ 10 dB). The EVM is under 4.5% for P_{out} up to 22.3 dBm with the maximum overall PAE of 33%. The EVM, gain, and overall PAE were also measured for the LTE 16QAM 5-MHz signal at 2.4 GHz (PAR $\sim$ 7 dB), as shown in Fig. 20. Under the EVM limit of 12.5% for LTE, the ET-based PA was able to produce 24.3-dBm output power (i.e., at $P_{1\mathrm{dB}}$) with an impressive overall PAE of 42%. The PAE

TABLE II
SUMMARY AND COMPARISON OF OUR MONOLITHIC ET-BASED PA SYSTEM WITH OTHER STATE-OF-THE-ART ET/EER PA AND/OR TX DESIGNS

	Freq. (GHz)	Gain (dB)	Avg. P_{out} (dBm)	[1]Overall PAE	[2]EVM	Signal BW (MHz)	Modulation	[3]PD	Technology
[14]	2.4	11	20	28%	5%	20	WLAN 64QAM	Yes	0.18 μm SiGe BiCMOS
[15]	1.88	27.8	29	46%	---	3.84	WCDMA	No	PA: 2 μm InGaP/GaAs
	1.88	27.9	23.9	34.3%	2.98%	5	WiMAX 64QAM	No	[4]EM: 0.13 μm CMOS
[16]	1.75	---	23.8	22%	1.69%	0.384	EDGE	Yes	0.18 μm CMOS
[17]	2.4	6.5	19	28%	2.8%	20	WLAN 64QAM	Yes	Discrete PA/EM
[18]	2.535	25	27.2	36.4%	---	10	LTE 16QAM	No	PA: 2 μm InGaP/GaAs EM: 65 nm CMOS
[19]	2.0	---	19.6	22.6%	2.5%	20	WLAN 64QAM	No	0.13 μm CMOS
[20]	1.95	---	28	46%	---	3.84	WCDMA	No	PA: GaAs EM: 0.18 μm CMOS
[21]	0.88	---	20	45%	---	0.384	EDGE	No	PA: 0.18 μm SiGe BiCMOS EM: discrete COTS
[22]	1.95	---	19	31%	2.1%	1.23	CDMA2000 QPSK	Yes	GaAs
[26]	1.56	---	14.7	8.9%	4.6%	20	WLAN 64QAM	No	0.18 μm CMOS
[27]	1.92	---	15.3	22%	1.5%	5	WiMAX 64QAM	Yes	0.13 μm SOI-CMOS
[28]	2.4	---	14	18%	4%	20	WLAN 64QAM	No	65 nm CMOS
[38]	1.88	24.62	24.22	38.6%	3.64%	5	WiBro 16QAM	No	PA: 2 μm InGaP/GaAs EM: 0.13 μm CMOS
[40]	0.9	---	27.8	34%	---	3.84	WCDMA	Yes	0.18 μm CMOS
This work	2.4	16	22.3	33%	4.2%	5	WiMAX 64QAM	No	0.35 μm SiGe BiCMOS
	0.8	22.8	23.5	43%	3.8%	5	LTE 16QAM	No	
	1.75	19.5	24.2	43%	4.8%				
	2.4	16.3	24.3	42%	5%				

Note: 1. The overall PAE includes the power consumption of the envelope modulator.
2. The EVM specs are 5% and 12% for WiMAX 64QAM standard and LTE 16QAM standard, respectively
3. PD: predistortion; 4. EM: envelope modulator.

and output power for WiMAX is lower than the case of LTE due to the higher PAR of the WiMAX signals. Moreover, our ET-based PA system can also support multiband applications. Fig. 21 shows the measured performances of the ET-based PA at 0.8/1.75/2.4 GHz using the LTE 16QAM 5-MHz input signal. The $P_{1\mathrm{dB}}$ output power is 23.5/24.2/24.3 dBm with PAE values of 43%/43%/42% and EVM values of 3.8%/4.8%/5%.

B. Linearity Enhancement of ET Technique

To demonstrate the linearity improvement of the cascode PA by using our ET technique, the cascode PA was also tested with a fixed supply voltage. The WiMAX 64QAM modulation was utilized for this comparison due to its more stringent linearity specs and higher PAR than that of the LTE 16QAM. Fig. 22 compares the EVM of the ET-based PA system and the fixed-supply PA ($V_{CC} = 3.6\ \mathrm{V}/4.2\ \mathrm{V}$) measured with the WiMAX 64QAM 5-MHz signal at 2.4 GHz. The EVM of the ET-based PA is lower than that of the fixed-supply PA when the output power is below 23 dBm (i.e., $P_{1\mathrm{dB}}$ of the ET-based PA system). The output spectra of the ET-based PA and the fixed-supply PA ($V_{CC} = 4.2\ \mathrm{V}$) are plotted in Fig. 23. Our ET-based PA passed the stringent WiMAX spectral mask with margins at close to its $P_{1\mathrm{dB}}$. For the fixed-supply PA, even though it was backed off by 7 dB from its $P_{1\mathrm{dB}}$, its adjacent channel power ratio (ACPR) was still higher than that of the ET-based PA system, especially at 2.5–8-MHz offset from the center frequency.

Table I summarizes the performances of our ET-based PA and the fixed-supply PA for both the WiMAX spectral mask and EVM spec (i.e., 5%). Even though the fixed-supply PA reaches 48% PAE at the $P_{1\mathrm{dB}}$ of 25 dBm, the maximum linear P_{out} is only 18 dBm (i.e., ∼7-dB back-off from $P_{1\mathrm{dB}}$), resulting in only 22% PAE. Once the P_{out} is above 18 dBm, it will first violate the WiMAX spectral mask (see Fig. 23). On the other hand, our ET-based PA can operate at close to its $P_{1\mathrm{dB}}$ while meeting the stringent WiMAX linearity specs with margins. The overall PAE of the entire ET-based PA system is 33%, which is 11% higher than the fixed-supply PA at the maximum linear P_{out}. Note that the $P_{1\mathrm{dB}}$ of our ET-based PA system is lower than that of the fixed supply PA (i.e., 23 versus 25 dBm). This is commonly seen in supply modulated PAs due to the gain compression at low supply voltages [14], [37]. Similar linearity performances were observed for the LTE 16QAM modulations as well, but with both higher linear P_{out} and overall efficiency due to its lower PAR compared with that of WiMAX. The transmission spurious noise of our ET-based PA is less than −45 dBm/MHz. The spurious noise can be attenuated by the additional output filtering and/or switching noise-reduction techniques [43].

C. Performance Summary and Comparison

The performance summary of our monolithic ET-based PA system against other state-of-the-art ET/EER PA/TX designs is given in Table II. It clearly shows that our design is among the highest efficiencies achieved in Si-based ET/EER PA/TX systems, approaching those of III-V based designs, such as [15], [18], [20], and [38]. This broadband high-efficiency performance makes our ET-based PA very attractive for future highly integrated TX systems, especially those of multiband mobile WiMAX and 3GPP LTE applications. Note this work has not yet utilized any predistortion. By adopting the state-of-the-art digital predistortion (DPD), the EVM and ACPR can possibly be improved by 3%–5% and 5–10 dB, respectively [44]. This is especially useful for WiMAX, as P_{out} of our ET-based PA can

be pushed beyond $P_{1\mathrm{dB}}$, leading to an overall PAE of $\sim$38% (see Fig. 19). We also expect that the power consumption of the digital baseband processor can be made reasonable low for mobile communication devices (e.g., the baseband processor only dissipated 1.1% of the entire power in [26]).

V. Conclusion

We have presented an ET-based cascode PA with an integrated envelope modulator for potential wideband wireless applications. The extensive analysis of what is necessary to achieve integration and corresponding circuitry caveats has been discussed. The self-biased differential cascode PA was modulated by the envelope-shifting method to improve the system linearity. The entire ET-based PA system achieved an overall PAE of 33% at P_{out} of 22.3 dBm for the WiMAX 64QAM signal and an overall PAE of 42% at P_{out} of 24.3 dBm for the LTE 16QAM signal (both at 2.4 GHz). Additionally, our ET-based PA presented a highly efficient multiband characteristic for LTE at 0.8/1.75/2.4 GHz. Without using any predistortion techniques, the ET-based PA satisfied the WiMAX spectral mask and EVM spec at close to its $P_{1\mathrm{dB}}$. As a comparison, the conventional fixed-supply PA required 7-dB back-off to pass the WiMAX linearity spec, resulting in 10% lower PAE and 4-dB lower P_{out} than the ET-based PA. Our monolithic ET-based PA system was fabricated in the TSMC 0.35-μm SiGe BiCMOS process on a single die. The literature survey indicates that our design achieved one of the highest efficiencies for Si-based ET/EER PA/TX systems with high PAR wideband signals.

Acknowledgment

The authors are deeply grateful to the Industrial Technology Research Institute (ITRI), Hsinchu, Taiwan, and TSMC, Hsinchu, Taiwan, for integrated circuit (IC) fabrication. The authors would like to thank Dr. K. Chen, S. Wu and T.-Y. Yang, all with ITRI, for their valuable suggestions and discussions on the test bench setup. The authors would also like to thank Dr. K.-S. Lu, CEO of Diodes Inc., Plano, TX, for generously contributing and setting up the Keh-Shew Lu Regents Endowment Fund at Texas Tech University (TTU), together with the kind contributions from C. S. Lee, M. Chiang, and J. England (all formerly with Texas Instruments Incorporated), and the TTU Board of Regents. The authors would also like to thank Dr. K.-S. Lu for underwriting the National Cheng-Kung University (NCKU)–TTU dual-degree exchange program sponsored by Diodes Inc. The authors also extend thanks to Prof. T. J. Liang, Prof. P.-C. Chung, and various faculty members of the Department of Electrical Engineering, NCKU, Tainan, Taiwan, for their kind support of the NCKU–TTU dual-degree exchange program.

References

[1] P.-C. Wang, C.-J. Chang, W.-M. Chiu, P.-J. Chiu, C.-C. Wang, C.-H. Lu, K.-T. Chen, M.-C. Huang, Y.-M. Chang, S.-M. Lin, K.-U. Chan, Y.-H. Lin, and C.-C. Lee, "A 2.4 GHz fully integrated transmitter front end with +26.5-dBm on-chip CMOS power amplifier," in *IEEE Radio Freq. Integr. Circuits Symp. Dig.*, Jun. 2007, pp. 263–266.

[2] F. Carrara, C. D. Presti, A. Scuderi, C. Santagati, and G. Palmisano, "A 3W 55% PAE CMOS PA with closed-loop 20:1 VSWR protection," in *IEEE Int. Solid-State Circuits Conf. Tech. Dig.*, Feb. 2007, pp. 80–81.

[3] I. Aoki, S. D. Kee, D. B. Rutledge, and A. Hajimiri, "Fully integrated CMOS power amplifier design using the distributed active-transformer architecture," *IEEE J. Solid-State Circuits*, vol. 37, no. 3, pp. 371–383, Mar. 2002.

[4] O. Degani, F. Cossoy, S. Shahaf, D. Chowdhury, C. D. Hull, C. Emanuel, and R. Shmuel, "A 90 nm CMOS power amplifier for 802.16e (WiMAX) applications," in *IEEE Radio Freq. Integr. Circuits Symp. Dig.*, Jun. 2009, pp. 373–376.

[5] D. H. Lee, C. Park, J. Han, Y. Kim, S. Hong, C.-H. Lee, and J. Laskar, "A load-shared CMOS power amplifier with efficiency boosting at low power mode for polar transmitters," *IEEE Trans. Microw. Theory Tech.*, vol. 56, no. 7, pp. 1565–1574, Jul. 2008.

[6] Y. Kim, B.-H. Ku, C. Park, D. H. Lee, and S. Hong, "A high dynamic range CMOS RF power amplifier with a switchable transformer for polar transmitters," in *IEEE Radio Freq. Integr. Circuits Symp. Dig.*, Jun. 2007, pp. 737–740.

[7] C. Park, Y. Kim, H. Kim, and S. Hong, "A 1.9-GHz CMOS power amplifier using three-port asymmetric transmission line transformer for a polar transmitter," *IEEE Trans. Microw. Theory Tech.*, vol. 55, no. 2, pp. 230–238, Feb. 2007.

[8] D. Chowdhury, C. D. Hull, O. B. Degani, Y. Wang, and A. M. Niknejad, "A fully integrated dual-mode highly linear 2.4 GHz CMOS power amplifier for 4G WiMAX applications," *IEEE J. Solid-State Circuits*, vol. 44, no. 12, pp. 3393–3401, Dec. 2009.

[9] K. H. An, D. H. Lee, O. Lee, H. Kim, J. Han, W. Kim, C.-H. Lee, H. Kim, and J. Laskar, "A 2.4 GHz fully integrated linear CMOS power amplifier with discrete power control," *IEEE Microw. Wireless Compon. Lett.*, vol. 19, no. 7, pp. 479–481, Jul. 2009.

[10] G. Liu, P. Haldi, T.-J. K. Liu, and A. M. Niknejad, "Fully integrated CMOS power amplifier with efficiency enhancement at power back-off," *IEEE J. Solid-State Circuits*, vol. 43, no. 3, pp. 600–609, Mar. 2008.

[11] V. Krishnamurthy, K. Hershberger, B. Eplett, J. Dekosky, H. Zhao, D. Poulin, R. Rood, and E. Prince, "SiGe power amplifier ICs for 4G (WiMAX and LTE) mobile and nomadic applications," in *IEEE Radio Freq. Integr. Circuits Symp. Dig.*, May 2010, pp. 569–572.

[12] J. Lopez, Y. Li, J. D. Popp, D. Y. C. Lie, C. C. Chuang, K. Chen, S. Wu, T.-Y. Ying, and G.-K. Ma, "Design of highly efficient wideband RF polar transmitter using the envelope-tracking technique," *IEEE J. Solid-State Circuits*, vol. 44, no. 9, pp. 2276–2294, Sep. 2009.

[13] T. Sowlati, D. Rozenblit, R. Pullela, M. Damgaard, E. McCarthy, D. Koh, D. Ripley, F. Balteanu, and I. Gheorghe, "Quad-band GSM/GPRS/EDGE polar loop transmitter," *IEEE J. Solid-State Circuits*, vol. 39, no. 12, pp. 2179–2189, Dec. 2004.

[14] F. Wang, D. F. Kimball, D. Y. C. Lie, P. M. Asbeck, and L. E. Larson, "A monolithic high-efficiency 2.4-GHz 20-dBm SiGe BiCMOS envelope-tracking OFDM power amplifier," *IEEE J. Solid-State Circuits*, vol. 42, no. 6, pp. 1271–1281, Jun. 2007.

[15] J. Choi, D. Kim, D. Kang, and B. Kim, "A polar transmitter with CMOS programmable hysteretic-controlled hybrid switching supply modulator for multistandard applications," *IEEE Trans. Microw. Theory Tech.*, vol. 57, no. 7, pp. 1675–1686, Jul. 2009.

[16] P. Reynaert and M. S. J. Steyaert, "A 1.75-GHz polar modulated CMOS RF power amplifier for GSM-EDGE," *IEEE J. Solid-State Circuits*, vol. 40, no. 12, pp. 2598–2608, Dec. 2005.

[17] F. Wang, D. F. Kimball, J. D. Popp, A. H. Yang, D. Y. C. Lie, P. M. Asbeck, and L. E. Larson, "An improved power-added efficiency 19-dBm hybird envelope elimination and restoration power amplifier for 802.11g WLAN application," *IEEE Trans. Microw. Theory Tech.*, vol. 54, no. 12, pp. 4086–4099, Dec. 2006.

[18] D. Kim, J. Choi, D. Kang, and B. Kim, "High efficiency and wideband envelope tracking power amplifier with sweet spot tracking," in *IEEE Radio Freq. Integr. Circuits Symp. Dig.*, Jun. 2010, pp. 255–258.

[19] J. S. Walling, S. S. Taylor, and D. J. Allstot, "A class-G supply modulator and class-E PA in 130 nm CMOS," *IEEE J. Solid-State Circuits*, vol. 44, no. 9, pp. 2239–2347, Sep. 2009.

[20] K. Takahashi, S. Yamanouchi, T. Hirayama, and K. Kunihiro, "An envelope tracking power amplifier using an adaptive biased envelope amplifier for WCDMA handsets," in *IEEE Radio Freq. Integr. Circuits Symp. Dig.*, Jun. 2008, pp. 405–408.

[21] D. Y. C. Lie, J. Lopez, J. D. Popp, J. F. Rowland, G. Wang, G. Qin, and Z. Ma, "Highly-efficient monolithic class E SiGe power amplifier design at 900 and 2400 MHz," *IEEE Trans. Circuits Syst. I, Reg. Papers*, vol. 56, no. 7, pp. 1455–1466, Jul. 2009.

[22] C.-J. Li, C.-T. Chen, T.-S. Horng, J.-K. Jau, and J.-Y. Li, "High average-efficiency multimode RF transmitter using a hybrid quadrature polar modulator," *IEEE Trans. Circuits Syst. II, Exp. Briefs*, vol. 55, no. 3, pp. 249–253, Mar. 2008.

[23] F. H. Raab, "Idealized operation of the class E tuned power amplifier," *IEEE Trans. Circuits Syst.*, vol. CAS-24, no. 12, pp. 725–735, Dec. 1977.
[24] A. Mazzanti, L. Larcher, R. Brama, and F. Svelto, "Analysis of reliability and power efficiency in cascode class-E PAs," *IEEE J. Solid-State Circuits*, vol. 41, no. 5, pp. 1222–1229, May 2009.
[25] T. Sowlati and D. M. W. Leenaerts, "A 2.4-GHz 0.18-μm CMOS self-biased cascode power amplifier," *IEEE J. Solid-State Circuits*, vol. 38, no. 8, pp. 1318–1324, Aug. 2003.
[26] A. Kavousian, D. K. Su, M. Hekmat, A. Shirvani, and B. A. Wooley, "A digitally modulated polar CMOS power amplifier with a 20-MHz channel bandwidth," *IEEE J. Solid-State Circuits*, vol. 43, no. 10, pp. 2251–2258, Oct. 2008.
[27] C. D. Presti, F. Carrara, A. Scuderi, P. M. Asbeck, and G. Palmisano, "A 25 dBm digitally modulated CMOS power amplifier for WCDMA/EDGE/OFDM with adaptive digital predistortion and efficient power control," *IEEE J. Solid-State Circuits*, vol. 44, no. 7, pp. 1883–1896, Jul. 2009.
[28] D. Chowdhury, L. Ye, E. Alon, and A. M. Niknejad, "A 2.4 GHz mixed-signal polar power amplifier with low-power integrated filtering in 65 nm CMOS," in *Proc. IEEE Custom Integr. Circuits Conf.*, Sep. 2010, pp. 1–4.
[29] C.-H. Lin and H.-Y. Chang, "A high efficiency broadband class-E power amplifier using a reactance compensation technique," *IEEE Microw. Wireless Compon. Lett.*, vol. 20, no. 9, pp. 507–509, Sep. 2010.
[30] Y. Li, J. Lopez, D. Y. C. Lie, K. Chen, S. Wu, and T.-Y. Ying, "Efficiency enhancement and linearity trade-offs for cascode versus common-emitter SiGe power amplifiers in WiMAX polar transmitters," in *Proc. IEEE Int. Circuits Syst. Symp.*, May 2010, pp. 1915–1918.
[31] Y. Li, J. Lopez, D. Y. C. Lie, K. Chen, S. Wu, T.-Y. Yang, and G.-K. Ma, "Circuits and system design of RF polar transmitters using envelope-tracking and SiGe power amplifier for mobile WiMAX," *IEEE Trans. Circuits Syst. I, Reg. Papers*, vol. 58, no. 5, pp. 893–901, May 2011.
[32] G. Seegerer and G. Ulbricht, "EDGE transmitter with commercial GSM power amplifier using polar modulation with memory predistortion," in *IEEE MTT-S Int. Microw. Symp. Dig.*, Jun. 2005, pp. 1553–1556.
[33] B. J. Minnis, P. A. Moore, P. N. Whatmough, P. G. Blanken, and M. P. van der Heijden, "System-efficiency analysis of power amplifier supply-tracking regimes in mobile transmitters," *IEEE Trans. Circuits Syst. I, Reg. Papers*, vol. 56, no. 1, pp. 268–279, Jan. 2009.
[34] R. Shrestha, R. V. D. Zee, A. D. Graauw, and B. Nauta, "A wideband supply modulator for 20 MHz RF bandwidth polar PAs in 65 nm CMOS," *IEEE J. Solid-State Circuits*, vol. 44, no. 4, pp. 1272–1280, Apr. 2009.
[35] F. H. Raab, "Split-band modulator for Kahn-technique transmitters," in *IEEE MTT-S Int. Microw. Symp. Dig.*, Jun. 2004, pp. 887–890.
[36] J. Jeong, D. F. Kimball, M. Kwak, C. Hsia, P. Draxler, and P. M. Asbeck, "Wideband envelope tracking power amplifier with reduced bandwidth power supply waveform," in *IEEE MTT-S Int. Microw. Symp. Dig.*, Jun. 2009, pp. 1381–1384.
[37] N. D. Lopez, X. Jiang, D. Maksimovic, and Z. Popovic, "Class-E power amplifier in a polar EDGE transmitter," in *IEEE MTT-S Int. Microw. Symp. Dig.*, Jun. 2006, pp. 785–788.
[38] J. Choi, D. Kang, D. Kim, and K. Kim, "Optimized envelope tracking operation of Doherty power amplifier for high efficiency over an extended dynamic range," *IEEE Trans. Microw. Theory Tech.*, vol. 57, no. 6, pp. 1508–1515, Jun. 2009.
[39] Y. Li, J. Lopez, D. Y. C. Lie, K. Chen, S. Wu, and T.-Y. Yang, "A broadband SiGe power amplifier in an efficient polar transmitter using envelope-tracking for WiMAX," in *IEEE 11th Top. Silicon Monolithic Integr. Circuits in RF Syst. Meeting Dig.*, Jan. 2011, pp. 136–140.
[40] A. Shameli, A. Safarian, A. Rofougaran, M. Rofougaran, and F. D. Flaviis, "A two-point modulation technique for CMOS power amplifier in polar transmitter architecture," *IEEE Trans. Microw. Theory Tech.*, vol. 56, no. 1, pp. 31–38, Jan. 2008.
[41] J. N. Kitchen, I. Deligoz, S. Kiaei, and B. Bakkaloglu, "Polar SiGe class E and F amplifiers using switch-mode supply modulation," *IEEE Trans. Microw. Theory Tech.*, vol. 55, no. 5, pp. 845–856, May 2007.
[42] Y. Li, J. Lopez, P.-H. Wu, D. Y. C. Lie, K. Chen, S. Wu, and T.-Y. Yang, "A highly-efficient RF polar transmitter using SiGe power amplifier and CMOS envelope-tracking amplifier for mobile WiMAX," in *Proc. IEEE Int. VLSI Design, Automat., Test Symp.*, Apr. 2011, pp. 1–4.
[43] T. O'Sullivan, R. A. York, B. Noren, and P. M. Asbeck, "Adaptive duplexer implemented using single-path and multipath feedforward techniques with BST phase shifters," *IEEE Trans. Microw. Theory Tech.*, vol. 53, no. 1, pp. 106–114, Jan. 2005.
[44] I. Kim, Y. Woo, J. Kim, J. Moon, J. Kim, and B. Kim, "High-efficiency hybrid EER transmitter using optimized power amplifier," *IEEE Trans. Microw. Theory Tech.*, vol. 56, no. 11, pp. 2582–2593, Nov. 2008.

Yan Li (S'09) received the B.S. degree in electrical engineering from Southwest Jiao-Tong University, Chengdu, China, in 2007, the M.S. degree in electrical engineering from Texas Tech University (TTU), Lubbock, in 2009, and is currently working toward the Ph.D. degree at TTU.

His current research interests include RF circuits for mobile wireless communications, especially the highly efficient and linear RF TXs/PAs design.

Mr. Li was the recipient of the AT&T Chancellor's Endowed Fellowship of Texas Tech University, and the Best Student Paper Awards at the IEEE International Symposium on Circuits and Systems (ISCAS), Paris, France (2010) and IEEE Topic Meeting on Silicon Monolithic Integrated Circuits in RF Systems (SiRF), Phoenix, AZ (2011).

Jerry Lopez (S'07) received the B.S. and M.E. degrees from the University of California at San Diego (UCSD), La Jolla, in 2001 and 2005, respectively, and the Ph.D. degree in electrical engineering from Texas Tech University, Lubbock, in 2011.

He has with the Northrop Grumman Corporation, where he was involved with research and development involving the design of highly efficient PAs and polar modulators including custom RF integrated circuit (RFIC) design. He has also worked with the U.S. Navy, where he was a member of the RFIC Design Group. He is currently with the Department of Electrical and Computer Engineering, Texas Tech University. His research interests include the design of analog/RF integrated circuits such as highly integrated highly efficient CMOS PA/TXs and circuits and systems that are highly nonlinear.

Dr. Lopez was the recipient of the Northrop Grumman Fellowship and the National Science Foundation (NSF) Educational Fellowship.

Po-Hsing Wu was born in Changhua, Taiwan, in 1986. He received the B.S. degree in electrical engineering from National Cheng Kung University, Tainan, Taiwan, in 2008, and the M.S. degree in electrical engineering from Texas Tech University, Lubbock, in 2010.

He is currently an Analog IC Design Engineer with Diodes Taiwan Inc., Hsinchu, Taiwan. His research interests include analog integrated circuit and power converter design.

Weibo Hu received the B.S. degree in electrical engineering from the Harbin Institute of Technology, Harbin, China, in 2005, the M. S. degree in electrical engineering (with honors) from the Peking University, Beijing, China, in 2008, and is currently working toward the Ph.D. degree in electrical engineering at Texas Tech University, Lubbock.

His research interests are in the area of low-power analog and mixed-signal circuit design.

Ruili Wu (S'11) received the B.S. degree in electrical engineering from the Institute of Microelectronics, Tsinghua University, Beijing, China, in 2010, and is currently working toward the Ph.D. degree in electrical engineering at Texas Tech University, Lubbock.

His current research concerns the design of integrated PA circuits and system for highly efficient linear wideband polar TXs in LTE-like wireless applications.

Mr. Wu was the recipient of the AT&T Chancellor's Endowed Fellowship of Texas Tech University.

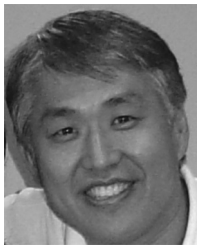

Donald Y. C. Lie (S'86–M'87–SM'00) received the M.S. and Ph.D. degrees in electrical engineering (minor in applied physics) from the California Institute of Technology, Pasadena, in 1990 and 1995, respectively.

He has held technical and managerial positions with companies such as Rockwell International, Silicon-Wave/RFMD, IBM, Microtune Inc., SYS Technologies, and the Dynamic Research Corporation (DRC). He is currently the Keh-Shew Lu Regents Chair Associate Professor (tenured) with the Department of Electrical and Computer Engineering, Texas Tech University, Lubbock. He is also an Adjunct Associate Professor with the Department of Surgery, Texas Tech University Health Sciences Center (TTUHSC). He is instrumental in bringing in multimillion dollar research funding and also designed real-world commercial communication products sold internationally. He has been a Visiting Lecturer with the Electrical and Computer Engineering Department, University of California at San Diego (UCSD), La Jolla, since 2002, where he taught upper division and graduate-level classes and was affiliated with the Center of Wireless Communications, UCSD, and co-supervised Ph.D. students. He was a Rotary International Scholar (1989–1990) and was awarded with an internship with Motorola Inc., sponsored by the Semiconductor Research Corporation (SRC) (1993–1994) and with the National Aeronautic and Space Administration (NASA) Jet Propulsion Laboratory (JPL) (1992–1993). He has authored or coauthored over 110 peer-reviewed technical papers and book chapters. He is the Area Editor-in-Chief for the *International Journal on Wireless and Optical Communications*. He is on the Editorial Board for the i-manager's *Journal on Electrical Engineering*. He has also been a Reviewer for many journals. He holds five U.S. patents. His research interests are low-power RF/analog integrated circuits and system-on-a-chip (SoC) design and test interdisciplinary research on medical electronics, biosensors, and biosignal processing.

Dr. Lie has served on the Executive Committee of the IEEE Bipolar/BiCMOS Circuits and Technology Meeting (BCTM), IEEE SiRF, IEEE MWSCAS, and on various Technical Program Committess (TPCs) for the IEEE RFIC Symposium, VLSI-DAT, PAWR, LiSSA, and DCAS committees. He has given numerous invited talks and short courses at IEEE conferences/workshops. He has been the associate editor of IEEE MICROWAVE AND WIRELESS COMPONENTS LETTERS. He was a guest editor of the IEEE JOURNAL OF SOLID-STATE CIRCUITS (JSSC) in 2009. He was the recipient of numerous awards from DRC, IBM, Rockwell. He and his students have been the recipients of several Best Graduate Student Paper Awards presented at international conferences in 1994, 1995, 2006, 2008 (twice), 2010 (twice), and 2011, and have also been awarded various scholarships.